Biosensors and Bioelectronics 49 (2013) 63–70

Contents lists available at SciVerse ScienceDirect

Biosensors and Bioelectronics

journal homepage: www.elsevier.com/locate/bios

Label-free monitoring of cell-based assays: Combining impedance analysis with SPR for multiparametric cell profiling

Michaelis S., Wegener J., Robelek R.*

Institute of Analytical Chemistry, Chemo- and Biosensors, University of Regensburg, Regensburg, Germany

ARTICLE INFO

Article history:
Received 25 March 2013
Received in revised form
22 April 2013
Accepted 23 April 2013
Available online 3 May 2013

Keywords:
Surface plasmon resonance
Electric cell-substrate impedance sensing
Real time monitoring
Label-free detection
Wholistic sensors
Whole cell biosensors

ABSTRACT

Label-free approaches to monitor cell-based assays provide an unprecedented, time-resolved and non-invasive view on the response of mammalian cells to chemical, biological or physical stimuli. The most widespread techniques are impedance analysis and optical sensing using evanescent waves like SPR. This study describes the combination of both in one experimental setup so that a given cell population can be monitored simultaneously for electrical and optical changes. The device is based on commercial SPR chips that are processed by photolithography to provide electrodes for impedance analysis and gold spots for surface plasmon excitation on the same substrate. Simultaneous recordings do not interfere with each other but provide independent, time-resolved information on cell shape changes (impedance) and dynamic mass redistribution (SPR) as they occur during exposure of the cells to drugs or toxins or along their normal life cycle. This study provides proof-of-concept experiments of the dual biosensor platform in two experimental settings: signals are recorded and analyzed (i) during cell attachment, spreading and differentiation of initially suspended cells and (ii) during the exposure of the mature cells to an actin cytoskeleton disrupting drug. Impedance and SPR recordings provide complementary information that can be used to trace and assign intracellular mechanisms of action.

1. Introduction

Label-free technologies to monitor cell-based assays are currently receiving considerable interest in drug development and toxicity screening as these techniques provide an entirely unbiased, time-resolved detection of the cellular response to a compound of interest. Among these, impedance analysis (e.g. ECIS™, Cell Key™) and evanescent wave-based optical techniques (e.g. EPIC™) are most widely applied even in industrial screening campaigns in 384well formats (Lee et al., 2008; Peters and Scott, 2009; Schroder et al., 2010; Scott and Peters, 2010). Impedimetric and evanescent wave-based assays are non-invasive so that the cell population under study can be monitored continuously for hours, days and even weeks. Thus, unlike endpoint assay, these readout techniques mirror the dynamics of the cells and their response to a given stimulus.

Both approaches are based on very different physical principles and the individual information content is different but complementary (Scott and Peters, 2010). In impedance-based approaches the cells are grown on gold film electrodes deposited on the bottom of a cell culture dish. When cells attach and spread on the electrode surface, the electrochemical impedance of the electrodes increases as the dielectric cell bodies impede current flow from the electrode into the bulk medium. The current has to bypass the cell bodies rendering the measured impedance sensitive to electrode coverage on the one hand and cell shape on the other. Any cell shape change leads to a corresponding change in the geometry of the current pathways and, thus, the recorded impedance. Accordingly, impedance-based approaches can be applied to a great number of different assays since it is well-known that cell shape is extraordinarily sensitive to any changes in cell metabolism and environment. The term *electric cell-substrate impedance sensing* (ECIS) has been introduced for this technology throughout the literature and as the brand name for the first commercial instrument (Giaever and Keese, 1993). During the last decade several different assays have been developed ranging from simple cytotoxicity studies to monitoring apoptosis or the stimulation of cell-surface receptors, like G-protein coupled receptors (GPCRs) (Arndt et al., 2004; Opp et al., 2009; Wegener et al., 1999).

The optical assays are based on generating an evanescent electric field along the growth substrate, which is affected by the refractive index within the first 100–200 nm perpendicular from the surface. Whenever the refractive index changes, the readout signal changes. Thus, these optical assays are sensitive to changes in mass distribution within the sensitive layer close to the substrate surface. The term has been established that evanescent wave-based optical techniques report on 'dynamic mass redistribution' induced inside the cell body or outside (Lee et al., 2008). There are several means to generate the evanescent wave. The device with the longest history is *surface plasmon resonance* analysis (SPR). In SPR a laser beam is directed to the interface between a glass substrate and a gold surface with an angle of

* Corresponding author. Tel.: +49 941 943 4048; fax: +49 941 943 4491.
E-mail address: rudolf.robelek@chemie.uni-regensburg.de (R. Robelek).

0956-5663/$ - see front matter © 2013 Elsevier B.V. All rights reserved.
http://dx.doi.org/10.1016/j.bios.2013.04.042

incidence that is greater than the angle of total reflection. When the resonance conditions are met, the evanescent field of the transmitted light excites a surface plasmon in the gold film that travels along the growth surface. The refractive index close to the surface determines the amount of energy trapped in the plasmon and, thus, the intensity of the reflected light. SPR has been used extensively to study molecular adsorption reactions at the solid–liquid interface and just recently it has been applied to study cell-based assays (Chabot et al., 2009; Robelek, 2009; Vala et al., 2013). Another way of realizing an evanescent wave close to the surface relies on optical gratings integrated into the surface of the growth substrate. The grating works like an optical filter such that polychromatic incident light is reflected as monochromatic light. The wavelength of the reflected light depends on the refractive index close to the surface as the filtering principle is also based on traveling evanescent waves with precisely defined resonance conditions (Lee et al., 2008). The technique has been applied extensively to study the activation of G-protein coupled receptors and it turned out to be extraordinarily helpful in assigning the associated signal transduction pathways (Schroder et al., 2010).

A combination of both techniques, impedance and SPR, has been successfully applied to numerous studies of molecular adsorption reactions at the solid–liquid interface in the past (Terrettaz et al., 1993). But to the best of our knowledge a combined impedance/SPR biosensor approach has never been applied to the analysis of living cells so far.

Comparing both techniques from a technical perspective reveals that impedance-based approaches integrate over the entire cell body as the current has to travel through or around the cells to reach the counter electrode. The optical devices based on evanescent fields are only sensitive to changes that occur close to the surface within the first 100–200 nm dependent on the excitation wavelength (Scott and Peters, 2010). Thus, the information from both devices is complementary and it seems highly desirable to develop combined sensors to record both signals from one and the same cell population. Such a combined, dual sensing device may overcome one of the limitations of these label-free approaches: the lack of molecular specificity. It is noteworthy that cell shape changes and dynamic mass redistribution are very general indicators for a cellular response and sometimes hard or even impossible to interpret on a molecular scale. A combination of both techniques in one experimental setup will increase the information depth and provide more specific time profiles that may allow for a more robust data analysis.

This study describes the design and performance of an experimental setup to monitor living animal cells simultaneously by non-invasive impedance readings (ECIS) and SPR recordings. The device is based on commercially available SPR substrates coated with a 45 nm gold layer that was processed by photolithography to hold a pair of electrodes for impedance readings and locally distinct areas for plasmon excitation and SPR detection. The experimental data shows that neither of the two measuring modes affects the other. By studying the time course of adhesion, spreading and polarization of initially suspended epithelial cells, the added-value of the dual sensor is demonstrated. Similarly, the biological response of the cells to the mycotoxin cytochalasin D (CD) is monitored with the dual sensor, providing a more comprehensive, spatially-resolved understanding of the functional changes occurring in the cells upon exposure to CD.

2. Materials and methods

2.1. Cell culture

All experiments were performed using the epithelial cell line MDCK II (Madin-Darby canine kidney, strain II). For stock cultures the cells were grown to confluence in standard cell culture flasks using Minimal Essential Medium (MEM-Earle) with 1 g/L D-glucose (Sigma-Aldrich, Steinheim, Germany), 5% (v/v) fetal calf serum, 4 mM L-glutamine and 100 μg/mL penicillin/streptomycin. The cultures were kept in an ordinary humidified cell incubator at 37 °C and 5% CO_2. The culture medium was exchanged twice a week. Routine subcultivation was performed by standard trypsinization protocols using 0.25% (w/v) trypsin plus 1 mM EDTA.

The clean and dry sensor surface was sterilized by exposure to an argon plasma (60 s) prior to cell inoculation. The sensor surface was inoculated with 450.000 cells/cm^2 in serum-containing, CO_2-independent buffer medium made up from PBS^{++} (phosphate buffered saline with 0.5 mM Mg^{2+} and 1 mM Ca^{2+}) supplemented with 1 g/L D-glucose, 5% (v/v) fetal calf serum, 4 mM L-glutamine and 100 μg/mL penicillin/streptomycin (= PBS^{++} complete buffer).

2.2. Preparation of the dual biosensor surfaces

The dual sensor platform was realized by implementing both techniques, ECIS and SPR, on a single sensor chip. ECIS–SPR chips were prepared from high refractive index glass slides (2.5 cm × 2.5 cm) covered with a 5 nm chromium bottom and a 45 nm top gold layer. The metal layers were subsequently structured by photolithography and wet etching. The positive photoresist AZ ECI 3027 (MicroChemicals, Ulm, Germany) was applied to the sensor by spin-coating at 3000 rpm using the manual spin coater WS-400-6NPP-LITE (Laurell Technologies Corporation, North Wales, USA). After soft bake, exposure to UV light through a corresponding mask, development of the UV-exposed areas and subsequent iodine/iodide-based etching of gold, the remaining photoresist was removed by washing with acetone. The sensors were then thoroughly washed with deionized water and dried at ambient conditions. In order to guarantee gold electrodes with a well-defined surface area and to prevent that other parts of the gold film than the actual electrodes contribute to the electrochemically active area, the contact paths were electrically insulated against the bulk electrolyte with positive photoresist by adding a second spin-coating and photolithographic step. Here, the adhesion promoter TI-Prime (MicroChemicals, Ulm, Germany) was spin-coated on the substrate surface before the photoresist was applied in order to improve resist adhesion after hard bake.

After finishing the sensor layout, a PDMS spacer (Sylgard 184 silicone elastomer kit, Dow Corning, Michigan, USA) forming a cell culture compatible flow cell was glued on top of the sensor using a non-toxic silicone adhesive (*Master fix Aquarium Silikon*, Warenimport und Handels GmbH, Vienna, Austria). The silicone glue was allowed to cure for about 24 h. The resulting sensor surface (Fig. 1) featured a combined measurement area consisting of two individually addressable small circular ECIS working electrodes (Ø~1 mm) and one large counter electrode, which was used as an SPR measurement area at the same time. Electrodes and SPR sensor spots were housed in a common fluid volume of about 500 μL as shown in Fig. 1.

2.3. Experimental setup of the dual biosensor platform

The new biosensor platform, as depicted in Fig. 1, combined the requirements for SPR and ECIS recordings in one experimental setup. The individual readouts from both techniques provide the optical and electrical properties of the cells on the sensor chip simultaneously.

2.3.1. SPR measurement

SPR measurements were performed with a Biosuplar 400T SPR system (MiviTec GmbH, Sinzing, Germany) at 37 °C. Prior to

assembling the experimental setup, sensor chip and flow cell were sterilized by an argon plasma treatment for 60 s (Harrick Plasma, New York, USA). The dual sensor chip was mounted to a F61-glass prism of the Biosuplar system using an appropriate immersion oil (RI = 1.61; Cargille, New Jersey, USA). The flow cell was covered with an acryl glass lid providing in- and outlet ports for the liquid handling via a syringe pump. After filling the system with PBS^{++} complete buffer a standard angle scan was performed to localize the reflectivity minimum angle. Subsequently, the SPR system was run in kinetic measurement mode, where changes in reflectivity (*ΔReflectivity*) were recorded over time (*t*) at a constant SPR observation angle. During the whole kinetic SPR measurement the observation angle was fixed to the value where the reflectivity minimum of the initial angle scan was located. This kinetic measurement mode was preferred over repeated angle scans for two reasons even though the latter would provide a precise determination of the minimum reflectivity angle: (i) The time resolution of the kinetic measurement mode is higher than in angle scan mode, so that even fast cellular processes can be monitored in real time. (ii) To study the attachment and spreading of initially suspended cells to the growth surface requires a constant horizontal position of the chip but no continuous tilting. Only in kinetic but not in angle scan mode the sensor surface remains horizontal. Before any measurement the system was equilibrated until a stable baseline was established.

2.3.2. ECIS measurement

For time-resolved impedimetric monitoring of the same cell population the two working electrodes and the counter electrode on the sensor chip were electrically connected to the impedance analyzer. A relay allowed switching between the two working electrodes. Relay and impedance analyzer were controlled by an ordinary PC. To acquire impedance data, the continuous wave impedance analyzer (Solartron Instruments SI-1260, Farnborough, UK) applied a non-invasive AC voltage of 30 mV (rms) to a working electrode/counter electrode couple. Measurements were performed at 61 designated frequencies (1 Hz–1 MHz) equally spaced on a logarithmic scale. The associated current was measured phase-sensitively and provided the complex impedance of the system as a function of frequency.

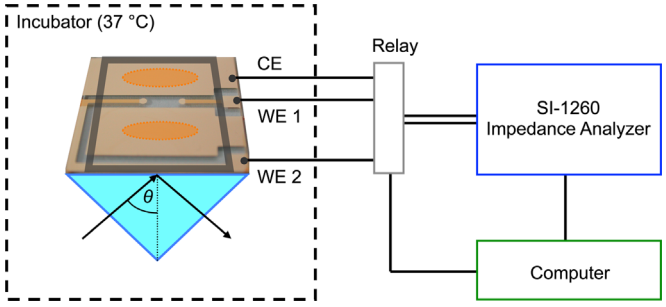

Fig. 1. Experimental setup to perform simultaneous SPR and ECIS measurements. The sensor chip is mounted on a high refractive index prism through which the laser beam is coupled into the gold surface for SPR recordings (orange fields). For ECIS recordings the electrodes – one working electrode (WE) and the bigger counter electrode (CE) – are connected to an impedance analyzer via a computer-controlled relay switch, which allows addressing the two different working electrodes. A PDMS chamber glued on the sensor chip serves as cell culture vessel.

2.4. Time-resolved monitoring of cell attachment and spreading as well as cell–cell junction formation

Suspensions of MDCK II cells in PBS^{++} complete buffer were routinely prepared from confluent cell layers by standard trypsinization protocols and diluted to a final concentration of 450.000 cells/cm^2. This inoculum provided a complete coverage of the entire sensor surface just by cell adhesion without the necessity of further cell division. 1 ml of cell suspension was used to completely exchange the flow cell buffer volume with a constant flow rate of 100 μL/min. After flow was stopped, the system was kept undisturbed and the reflectivity changes were recorded for 20 h with a time resolution of 3 s. SPR data was recorded using the manufacturer's software. Fig. 2A shows typical SPR angle scans recorded with a prototype ECIS–SPR chip (cp. Fig. 1) with and without a confluent layer of MDCK cells.

Multi-frequency impedance spectra were recorded as described above, providing a time resolution of 2.3 min when two electrodes are monitored. The measured complex impedance was broken up into real (resistance) and imaginary (reactance) contributions along the entire spectrum and the frequency-dependent capacitance of the system was calculated from the reactance. Capacitance readings recorded above a certain threshold frequency are most sensitive to cell attachment and spreading as only high frequency current couples capacitively through the cell membranes (transcellular current pathway) instead of flowing around the cell bodies. Wherever the substrate is covered with a planar cell membrane, the total capacitance in this area equals a series combination of electrode and membrane capacitance ($1/C_{tot} = 1/C_{el} + 1/C_{cell}$) which is smaller than the electrode capacitance itself. Thus, when the cell membranes gradually flatten out on the electrode, the overall capacitance drops from values of a cell-free to those of a cell-covered electrode and mirrors the time course of cell spreading. For the electrode sizes used here, capacitance readings at an AC frequency of 20 kHz are best suited to monitor the time course of cell attachment and spreading to the sensor surface (Michaelis et al., 2012; Wegener, 2010). The establishment of cell–cell contacts was monitored by recordings of the electrical impedance at a sufficiently low frequency in order to guarantee current flow

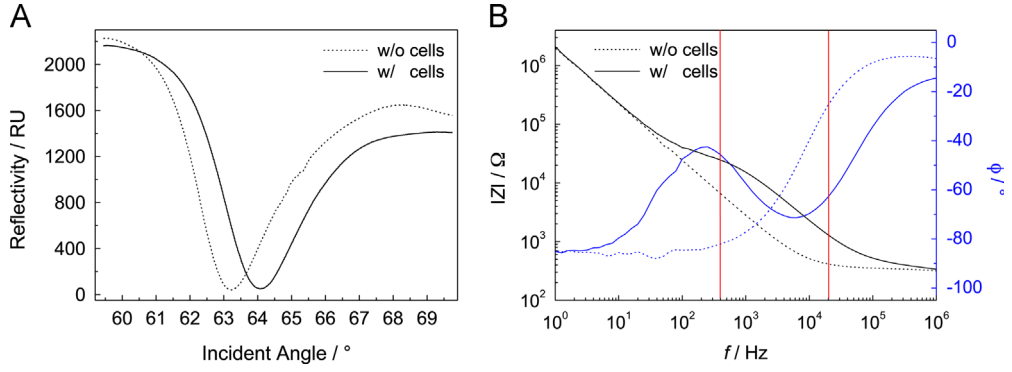

Fig. 2. Typical SPR angle scans (A) and Bode presentation of impedance (black curves) and phase spectra (blue curves) (B) as recorded with the combined ECIS–SPR setup for a sensor surface covered with (solid line) or without (dashed line) a confluent layer of MDCK II cells. The two monitoring frequencies are indicated by red vertical lines.

around the cells through the cell–cell junctions (paracellular current pathway). Here, the monitoring frequency was adjusted to 400 Hz to follow cell junction formation (Michaelis et al., 2012; Wegener, 2010). Fig. 2B shows typical impedance and phase spectra of the electrode layout of a prototype ECIS–SPR chip (cp. Fig. 1) with and without a confluent monolayer of MDCK cells.

2.5. Time-resolved monitoring of cytoskeleton disruption

We used cytochalasin D (CD) as a well-defined model compound to study the responses of the two sensors to cytoskeletal destructions. CD is a membrane-permeable fungal toxin and a potent inhibitor of g-actin polymerization into growing filaments while leaving depolymerization unchanged. During exposure to CD the actin filaments shorten and eventually disassemble completely leaving actin aggregates behind.

After a confluent MDCK monolayer was established on the sensor surface and the electrical properties remained stationary (~20 h) the cells were treated with 5 μM CD dissolved in PBS^{++} complete buffer while continuously monitoring the cell response by simultaneous SPR and ECIS measurements.

2.6. Microscopic documentation of cytoskeleton disruption

According to time-resolved ECIS and SPR recordings the response of the cells to the exposure to CD is complete after less than 3 h. To document the associated changes in the actin cytoskeleton the MDCK cell layer was stained for microscopic documentation using TRITC-labeled phalloidin (tetramethylrhodamine isothiocyanate; ex./ em.: 540 nm/570 nm) and compared to an untreated control cell layer. Cells on the sensor chip were carefully washed twice with PBS^{++} and subsequently fixed with 4% (w/v) paraformaldehyde in PBS^{++} for 10 min. After removal of the fixative and additional washing steps the cells were permeabilized with the non-ionic detergent Triton X-100 (0.2% (v/v) in PBS^{++}) for 10 min since the phalloidin molecule cannot pass intact cell membranes. After two more washing steps the cells were incubated with 0.3 μg/mL TRITC-labeled phalloidin in PBS^{++} for 45 min in the dark. Finally, the sample was rinsed with PBS^{++} several times and fixed again with 4% (w/v) PFA for 10 min. Microscopic imaging was performed in PBS^{++} using the upright confocal laser scanning microscope Nikon Eclipse 90i (Nikon Instruments Europe, Amsterdam, Netherlands) and a 60 × (NA = 1.0) water immersion objective.

3. Results and discussion

3.1. Development and performance of the ECIS–SPR biosensor platform

The newly designed ECIS–SPR biosensor platform (Fig. 1) exhibits both, a coplanar electrode arrangement similar to the situation on a commercially available standard ECIS electrode array and a regular SPR substrate. To demonstrate suitability and performance of this dual biosensor, we pursued measurements in ECIS and SPR mode (i) of the cell-free, medium-covered sensor surface, (ii) during attachment and spreading of MDCK II cells (Madin-Darby canine kidney, strain II) and (iii) after a confluent monolayer of these cells had been established on the surface.

Similar measurements for cell-free and cell-covered gold surfaces have already been performed for either of the applied techniques individually in independent experiments (Lo et al., 1995; Robelek and Wegener, 2010) so that the overall spectral characteristics and characteristic values for signal shifts of impedance and phase (ECIS) and resonance angle (SPR) are well-known. Fig. 2 shows typical angle scans (Fig. 2A) and impedance/phase spectra (Fig. 2B) as recorded with the dual ECIS–SPR setup. Data for a cell-free surface, only incubated with cell culture medium, are compared to the same surface after a confluent monolayer of MDCK II cells was established. The excitation of surface plasmons is indicated by a dip in reflectivity at a specific angle of incidence, which is determined by the refractive index of the attached cells.

The recorded SPR scans (Fig. 2A) show a significant upward shift of the resonance angle by around 1° going from cell-free to cell-covered surfaces. The final value of the resonance angle for a cell-covered sensor surface amounts to 64.2°. These values are not significantly different from SPR readings obtained for cell-free and cell-covered chips in an SPR-only experiment using continuous gold surfaces for plasmon excitation (cp. Fig. S1 in supplementary material). We conclude from these observations that (i) MDCK II cells indeed form a confluent cell monolayer on the ECIS–SPR chips just as they do on the individual devices and (ii) neither the discontinuous gold surface with the ECIS electrode layout nor low-amplitude impedance recordings perturb SPR detection. The pool of our experimental SPR data indicates that the degree of surface coverage is linearly correlated with the shift of the SPR resonance angle (cp. Fig. S2 in supplementary material). The final value of the resonance angle for confluent cell monolayers turned out to be very reproducible. The pool of our data provides an average angle of $(64.3 \pm 0.1)^\circ$ for confluent MDCK II cells. When different cell types were studied by SPR, we did not find significantly different values for the cell-type specific resonance angle shift. Thus, it seems unlikely that the pure resonance angle shift contains cell-type specific information but is rather dominated by more general system parameters like, for instance, surface coverage with cells.

Fig. 2B compares the impedance (black curves) and phase spectra (blue curves) for a medium-covered electrode and the same electrode after a monolayer of MDCK II cells had been established on its surface. The cell-free electrode reveals a characteristic and well-known frequency dependence of the impedance (Arndt et al., 2004; Giaever and Keese, 1991; Wegener et al., 2000a). For high frequencies ($f > 10^5$ Hz) the total impedance of the system is frequency-independent as it is determined by the bulk resistance of the electrolyte. At lower frequencies ($f < 10^4$ Hz) the impedance of the electrode–electrolyte interface dominates the impedance spectrum, giving rise to a linear increase of impedance with decreasing frequency in this log–log presentation. This behavior is typical for gold film electrodes immersed in physiological fluids and very close to the behavior of an ideal capacitor (McAdams et al., 1995). The presence of cells on the electrode surface primarily affects the impedance spectrum at intermediate frequencies between 60 Hz and 10^5 Hz. At the high ($f > 10^5$ Hz) and low frequency end ($f < 10$ Hz) the spectra of a cell-free and a cell-covered electrode merge. The phase spectra are in line with this interpretation. The phase of the cell-free electrode is close to zero at high frequency as the spectrum is dominated by the electrolyte resistance. At low frequencies the phase value gets close to −90° which is typical for an almost ideally polarizable electrode like gold films in physiological buffers. The phase spectrum of the cell-covered electrode approaches the phase spectrum of the cell-free electrode at the high and low frequency end. The cell layer itself induces a shift of the phase spectrum along the frequency axis and a dispersion at intermediate frequencies. For the more interested reader Fig. S3 (Supplementary material) provides an additional plot of the frequency-dependent total impedance of a cell-free electrode in comparison to a cell-covered electrode in complex presentation with the imaginary part of the impedance (reactance) plotted as a function of the real part (resistance). Taken together, these spectral characteristics are

not significantly different from data recorded with commercial ECIS electrodes and they have been described by others before (Giaever and Keese, 1991, 1993; Wegener et al., 2000a). In complete agreement to the SPR measurements, the ECIS data confirm (i) the formation of a confluent MDCK II cell layer on the electrode surface and (ii) no perturbing influences of SPR detection on ECIS data recording. Thus, the two measurement modes are compatible with each other and can be performed in parallel without any noticeable influence on cell growth or cell behavior.

3.2. Simultaneous, time-resolved SPR and ECIS measurements of cell adhesion and differentiation

To learn more details about the information available from an ECIS–SPR dual sensor in comparison to individual and separate single sensor experiments, we conducted time-resolved measurements with both techniques during attachment and spreading of initially suspended MDCK II cells including the differentiation of the cells into a barrier-forming phenotype with tight junctions between adjacent cells (Wegener, 2003; Wegener and Galla, 1996). For this purpose, the ECIS–SPR sensor was assembled with the flow cell and mounted into the Kretschmann SPR configuration kept at 37 °C. The flow cell was filled with PBS^{++} complete buffer and left for an initial incubation time of 10 min to obtain sensor equilibration with the serum-containing buffer. Subsequently, an SPR angle scan was conducted to find the SPR resonance angle. The angle was fixed to the value that corresponded to the reflectivity minimum and reflectivity changes were recorded with time. A stable baseline was observed within 10 min. Impedance spectra of the medium-covered cell-free electrode were recorded in parallel. After baseline recording the flow cell was flushed with the cell suspension until a complete medium exchange was guaranteed. Thereafter, flow was stopped and cell attachment and spreading were followed in SPR and ECIS mode. Fig. 3 presents the kinetic SPR (A) and ECIS data (B) obtained after addition of the cell suspension at time zero. The time scale has been plotted logarithmically to get a more balanced perspective on early and later signal changes. 10 min after addition of the cell suspension the reflectivity begins to rise very rapidly (Fig. 3A) indicating substantial refractive index changes within the evanescent measurement field. This change in reflectivity mirrors the formation of specific, integrin-mediated cell-substrate contacts immediately followed by the onset of cell spreading. This conclusion is based on two observations: (i) in the presence of peptides (Arg–Gly–Asp–Ser=RGDS) that are known to inhibit the formation of specific cell-substrate contacts (Li et al., 2005; Ruoslahti and Pierschbacher, 1987; Yamada and Kennedy, 1984) this initial increase in reflectivity was not observed. The signal stayed rather constant and similar to a cell-free surface for more than 100 min, indicating that loosely attached, settled cells without specific interactions to surface-bound proteins do not reach the evanescent field to any significant extent (data not presented here). (ii) When the cells populate the surface in closest packing without spreading but in a rather spherical morphology, only 3% of the evanescent volume is occupied assuming a penetration depth of the evanescent wave of approx. 100 nm. Thus, closest packing of spherical cells cannot explain the experimental increase in reflectivity and cell spreading has to contribute to the signal.

In the experiment shown in Fig. 3A the slope of the curve is reduced significantly within 100 min after cell inoculation before it becomes independent of time 400 min after inoculation till the end of the observation period. We interpret the reduced slope between 100 and 400 min as the period when the cortical actin cytoskeleton maturates as will be discussed below. Constant values of reflectivity recorded after 400 min of experimental time

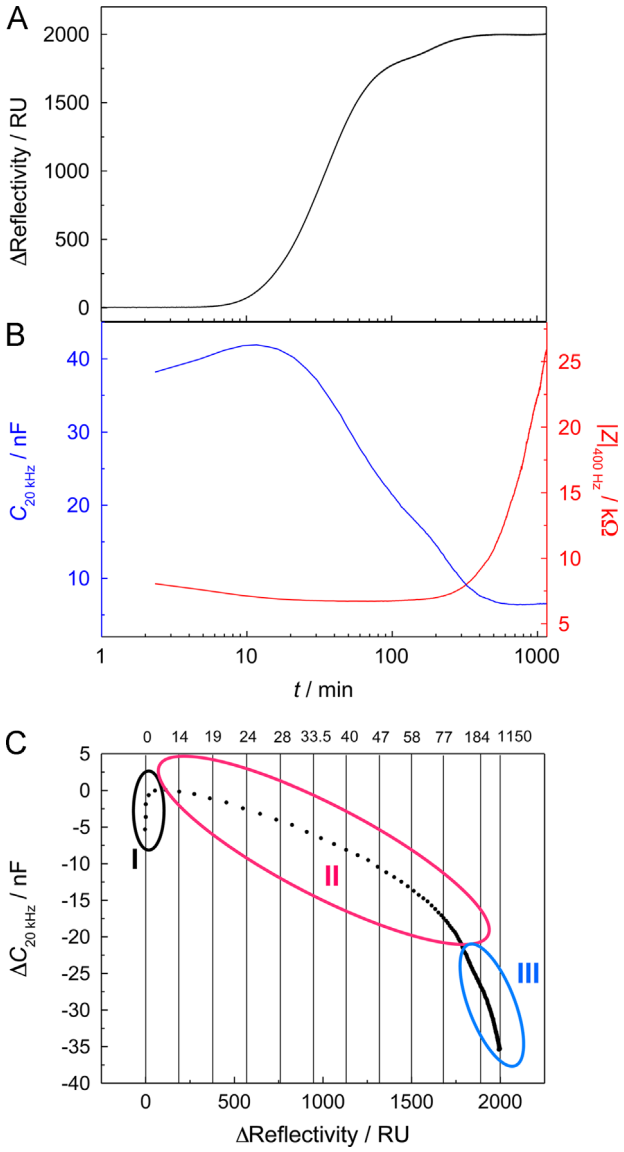

Fig. 3. Adhesion and differentiation kinetics of MDCK II cells monitored by SPR and ECIS readings. (A) Time course of the changes in reflectivity. (B) Time course of the electrode capacitance recorded at 20 kHz (blue curve) and the electrode impedance at 400 Hz (red curve). Cells were seeded in a density of 4.5×10^5 cells/cm^2 at time zero. (C) ΔC vs. Δ*Reflectivity* plot during cell adhesion and differentiation. The experimental time is indicated by vertical lines through the graph. The three phases of cell layer development (I=settling and formation of first cell-surface contacts, II=gradual spreading and III=differentiation) are marked with different colors.

indicate the establishment of a continuous cell monolayer without any open spaces on the surface and no significant molecular redistributions inside the cells close to the surface.

In ECIS mode, the time course of cell attachment and spreading of initially suspended MDCK II cells was followed by capacitance readings at an AC frequency of 20 kHz (Fig. 3B, blue curve). For this high frequency, it has been shown in the past that the decrease in total capacitance is linearly correlated with the coverage of the electrode surface with cells (Wegener et al., 2000b). Accordingly, during the lag phase between inoculation and early cell attachment (first 10 min) the capacitance is not reduced. The observed increase is, however, due to the rather slow electrochemical equilibration of the sensor surface. With the cells reaching the surface this positive drift of the capacitance is overruled by spreading of the cells upon the electrode which reduces the total capacitance from 40 down to 6 nF at this particular frequency in

two distinct steps: (i) between 10 and 100 min and (ii) between 100 and 400 min. Thus, the time course of capacitance decrease is very similar to the increase in reflectivity. The first phase of capacitance decrease is caused by cell spreading, the second by the establishment of a mature cytoskeleton and the formation of cell junctions as will be discussed below. Both quantities apparently mirror the spreading of the cells to the sensor surface from different perspectives. SPR monitors the change in refractive index close to the surface due to the spreading of cell bodies, whereas ECIS reads the gradual electrical blockade of the electrode by the dielectric plasma membranes. The entirely different physics behind the individual signal generation accounts for the individual aspects of the two time courses.

In addition, ECIS is capable of monitoring the formation of cell–cell junctions (tight and adherens junctions) along the experiment as a quantitative indicator of cell polarization and differentiation (Cereijido et al., 2000). At a sufficiently low monitoring frequency (here: 400 Hz) the current passes the cell layer on paracellular pathways and is impeded by the narrow cleft between adjacent cells and the barrier-forming cell–cell junctions at the apical pole. Fig. 3B shows the time course of the impedance at a frequency of 400 Hz directly after cell inoculation at time zero (Fig. 3B, red curve). The impedance does not change significantly during the first 200 min of the experiment. It is apparently insensitive to cell spreading. However, after spreading is complete, the impedance at 400 Hz increases continuously till the end of the experiment and the impedance time course mirrors the expression of cell–cell junctions. Comparing both time courses, it becomes obvious that the increase in $|Z|$ only starts after C has passed through 70% of its total change and has just progressed in its second phase of decline. This is entirely inline with predictions from a theoretical model for the impedance of cell-covered electrodes (Arndt et al., 2004; Giaever and Keese, 1991). If this model is applied to the electrode size, frequency and cell type used here, it returns a fractional capacitance shift of 80% due to cell attachment and spreading whereas the remaining 20% are provided by junction formation. Accordingly, the second phase of the capacitance time course mirrors the early phase of junction formation while this parameter is insensitive to junction maturation into a high resistant phenotype. Formation of the latter is completely mirrored in the impedance time course.

At this point it seems noteworthy to stress our way of analyzing the impedance raw data. In the literature many researchers use equivalent circuit modeling to extract the dielectric parameters of the system under study. In our previous work we have done the same for cell-covered gold film electrodes (Wegener et al., 1999; Wegener et al., 2000a). However, modeling the impedance raw data in order to extract the dielectric parameters of the cells on the electrode is only meaningful for confluent cell layers with no open spaces on the electrode surfaces. Otherwise the parameter estimates of the models are rather meaningless and cannot be interpreted. For the interested reader: we have analyzed the raw data of the experiment shown in Fig. 3 by an equivalent circuit consisting of a series combination of R (resistance of the bulk) and C (electrode capacitance) together with a parallel combination of R_{cl} (resistance of cell layer) and C_{cl} (capacitance of cell layer). As has been shown before (Wegener et al., 1999), the latter two represent the dielectric properties of the cell layer – when confluent. Fig. S4 shows the time course of C_{cl} and R_{cl} for the spreading experiment. Capacitance values are unrealistically high until the cell layer has formed within the first 200 min of the experiment. Only for $t > 200$ min the analysis returned a meaningful cell layer capacitance C_{cl} in the order of 1 μF/cm².

To avoid misinterpretation of fitted parameter estimates we have used a different approach in this and in other studies that does not rely on data fitting. By studying the time course of the complex impedance at different frequencies (in theory and experiment) during the establishment of a confluent cell monolayer starting from initially suspended cells and a cell-free electrode, we were able to identify those frequencies at which impedance, resistance or capacitance are particularly well-suited to zoom in on certain aspects of the cell body and monitor a given process without data modeling. We learned from those studies that spreading of cells can be most easily monitored by readings of the total capacitance above a threshold frequency of 10 kHz. At these frequencies the total capacitance of the system scales linearly with the gradual coverage of the electrode. Moreover, probing the cell–cell junctions requires the current to flow around the cell bodies on paracellular pathways – instead of capacitively running through the cells. At 400 Hz the total impedance change is dominated by tightening of the cell layer due to the formation of cell–cell junctions. Fig. S5 in the supplementary material shows the time courses of R_{cl} and $|Z|$(400 Hz) in the same diagram. Both curves show a very similar, almost identical time course supporting our approach to use well-selected raw data instead of fitted parameter estimates with uncertain interpretation.

Direct comparison of the time courses of the reflectivity (SPR) on the one hand and capacitance and impedance (ECIS) on the other hand, reveals that the second phase of reflectivity increase, the second phase of capacitance decrease and the onset of impedance increase occur roughly at the same time. Based on the above mentioned conclusions we therefore interpret the second phase of reflectivity increase as being caused by the rearrangement and maturation of the cortical actin close to the membrane during polarization and maturation of the spread cells. It is well-known that the actin cytoskeleton has to adopt certain morphological features and stabilize adherens junctions before the diffusion limiting tight junctions are formed (Wegener, 2003; Wegener and Galla, 1996).

Fig. 3C plots the change in capacitance as a function of the change in reflectivity. The experimental time is no longer represented on the axis but indicated by vertical lines through the graph. We can distinguish the three phases of cell layer development as discussed above. In phase I the cells settle down to the surface but neither of the two devices is capable of monitoring the simple settlement without the formation of specific cell-surface junctions of the ligand–receptor type. Phase II describes the gradual spreading of cells upon the electrode. Both signals are not linearly correlated to perfection in this phase as they are determined by physically different phenomena. The addition of mass to the volume defined by the evanescent wave causes the SPR signal to change, whereas an effective electrical blockade of the electrode causes the ECIS signal to adapt. Phase III describes the time period of cell differentiation when cell–cell junctions are formed. In this phase the reflectivity changes only slightly as only minor mass redistribution is associated with it, whereas the capacitance at 20 kHz is affected more prominently caused by the increasing electrical tightness of the cell layer.

3.3. Simultaneous, time-resolved SPR and ECIS measurements of cytoskeleton disruption

As a second proof-of-concept experiment we studied the response of a confluent MDCK II cell layer to the drug cytochalasin D (CD) with the dual biosensor. The membrane-permeable mycotoxin CD acts as a potent inhibitor of actin polymerization while depolymerization is unaffected. Thus, exposure to CD leads to a net contraction of actin fibers and their decomposition in actin aggregates (Flanagan and Lin, 1980). Confluent monolayers of MDCK cells were exposed to 5 μM CD while performing simultaneous SPR and ECIS measurements to follow the cellular response to actin cytoskeleton disruption.

The kinetic SPR measurement (Fig. 4A) shows a transient increase (spike) followed by a major decrease of the reflectivity signal upon addition of 5 μM CD, approaching new stationary values within 150 min. The change in reflectivity amounts to 500 response units. Compared to the signal increase from a cell-free to a cell-covered surface of approx. 2000 response units (Fig. 3A), the CD-induced reduction is just 25% of the total reflectivity change caused by the cells. This indicates that a significant mass redistribution occurs close to the surface as it is expected for actin filament degradation close to the membrane. However, the cell bodies remain on the surface as verified by microscopic inspection. Fig. 4B shows ECIS mode measurements of the cellular responses to CD. Again, we recorded the capacitance at 20 kHz as an indicator of electrode surface coverage and the impedance at 400 Hz to probe barrier-forming cell–cell contacts with time. Upon exposure to CD the time course of the impedance at 400 Hz reports on a massive and rather fast loss of cellular barrier function starting immediately after CD addition (arrow). The measured impedance decreases within 15 min and approaches the impedance of a cell-free electrode at this frequency, indicating that the paracellular current pathway has widened and cell junctions disassembled. This behavior has been described for these and other epithelial cells before (Madara et al., 1988; Wegener et al., 2000c) and CD is widely accepted as a potent modulator of epithelial barrier function, as tight junctions are directly linked to the actin cytoskeleton. The capacitance shows only a slight increase. This change in capacitance is consistent with the loss of cell junctions as its magnitude compares favorably with the change in capacitance during junction formation when the cells polarize (Fig. 3B). However, membrane integrity is obviously not significantly affected by the drug and the electrode surface remains covered with a confluent monolayer of spread cells. Otherwise capacitance values would have increased to more than 45 nF.

This data interpretation is backed up by fluorescent micrographs of MDCK cells with their actin cytoskeleton stained by TRITC-phalloidin before and after exposure to CD (Fig. 4C). The micrograph for the CD-treated cell layer (Fig. 4C2) shows that the actin network has condensed to actin aggregates but the cells remain attached and spread on the surface. In the untreated sample (Fig. 4C1) the cells express a junctional actin belt that follows the cell periphery and stabilizes cell-to-cell junctions. Moreover, the control cells express actin stress fibers running as parallel bundles along the lower, substrate-facing membrane. Both structures are completely disassembled upon exposure to CD. Control experiments in which the cell layer was treated with a corresponding amount of DMSO that was used as a solvent for CD did not show any parameter changes (data not shown).

Comparing the time courses of SPR and ECIS readings, it is obvious that the reflectivity changes slower than the impedance decreases. Here the reflectivity reports primarily on changes in actin filaments close to the lower membrane (stress fibers), while impedance readings report extremely sensitive on changes in the cell–cell junctions close to the apical pole of the cell for which the SPR technique is basically blind. The differences in both signals compare nicely to observations reported from quartz crystal microbalance (QCM) studies (Wegener et al., 2000c). The QCM technique is sensitive to micromechanical changes within the cells as long as they occur close to the substrate-facing membrane. QCM readings for the same cell type provide a very similar time course as SPR traces when the cells are exposed to 5 μM CD supporting our understanding of ECIS–SPR data. Moreover, Stevenson and Begg found that these two different actin subpopulations (actin belt vs stress fibers) are individually sensitive to CD (Stevenson and Begg, 1994). The actin belt was found to respond more sensitively to CD than the stress fibers close to the basal membrane. Taken together, the ECIS–SPR dual sensor provides a more comprehensive description of structural and functional changes that occur inside living cells when they are exposed to cytoskeleton active drugs. With the different spatial sensitivities and individual integration over the cell body, both techniques are

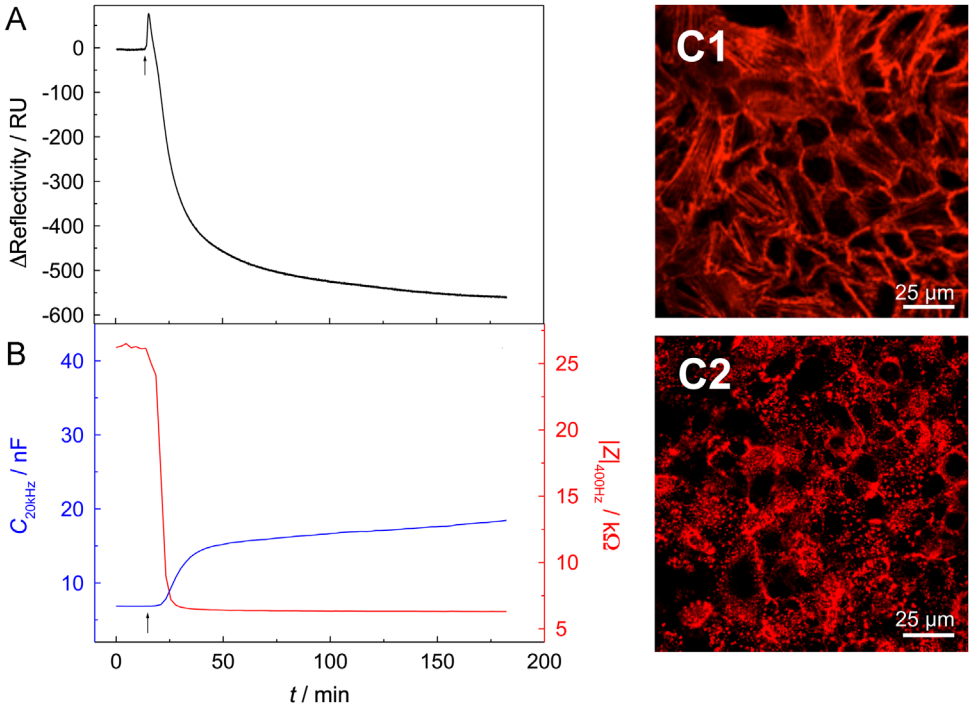

Fig. 4. Response of a confluent MDCK II cell layer to 5 μM cytochalasin D analyzed by simultaneous SPR (A) and ECIS measurements (B). Time course of the reflectivity change (A), the capacitance at 20 kHz (B, blue curve) and the impedance at 400 Hz (B, red curve) before and after CD addition (arrow). (C) shows confocal fluorescence micrographs of confluent MDCK II cells grown on the biosensor surface and stained for their actin cytoskeleton (with fluorescently labeled phalloidin) before (C1) and after (C2) exposure to CD (5 μM, 3 h). The focal plane was set to the basal cell membrane.

complementary to each other and the interpretation of the experimental data from one channel benefits from the outcome of the other. The additional information provided by dual biosensor devices may pave the way to a functional high content analysis of cell-based assays.

4. Conclusions

The ECIS–SPR dual biosensor provides the information of the two most prominent label-free techniques that are used nowadays to monitor cell-based assays. Both techniques have proven independently how useful they can be to follow the biological response to drugs or toxins in an entirely unbiased and integral approach. The individual time course data has been successfully interpreted as a fingerprint of a given bio-response and has been used to unravel the intracellular mechanism of action. The basis for fingerprint analysis and mechanistic studies is significantly broadened by combining these techniques so that characteristic profiles of physically different and complementary indicators can be obtained and analyzed. The ECIS–SPR dual biosensor represents such a combined sensor platform that can be tuned to report on different parts of the cell body and on different functional changes. As such it provides time-resolved information on dynamic mass redistribution and cell shape changes within one and the same cell population for subsequent data mining and data interpretation in two instead of only one dimension.

The proof-of-concept experiments shown in this manuscript have been focussed on cell attachment and spreading as well as cytoskeleton disassembly as initial test assays. In our ongoing research we are exploring the potential of the ECIS–SPR readout in assays addressing the cellular response after stimulation of G-protein coupled receptors (GPCRs). The combined approach will provide fingerprint data sets with improved information depth compared to the individual techniques and, thus, a stronger base to identify the associated signal transduction cascade(s) and to unravel functional selectivities of GPCR ligands.

Acknowledgments

The authors would like to thank Barbara Goricnik and Nadja Hinterreiter for their indispensable help and expertise with the cell cultures.

Appendix A. Supporting information

Supplementary data associated with this article can be found in the online version at http://dx.doi.org/10.1016/j.bios.2013.04.042.

References

Arndt, S., Seebach, J., Psathaki, K., Galla, H.J., Wegener, J., 2004. Biosensors and Bioelectronics 19 (6), 583–594.
Cereijido, M., Shoshani, L., Contreras, R.G., 2000. American Journal of Physiology—Gastrointestinal and Liver Physiology 279 (3), G477–482.
Chabot, V., Cuerrier, C.M., Escher, E., Aimez, V., Grandbois, M., Charette, P.G., 2009. Biosensors and Bioelectronics 24 (6), 1667–1673.
Flanagan, M.D., Lin, S., 1980. Journal of Biological Chemistry 255 (3), 835–838.
Giaever, I., Keese, C.R., 1991. Proceedings of the National Academy of Sciences 88 (17), 7896–7900.
Giaever, I., Keese, C.R., 1993. Nature 366 (6455), 591–592.
Lee, P.H., Gao, A., van Staden, C., Ly, J., Salon, J., Xu, A., Fang, Y., Verkleeren, R., 2008. Assay and Drug Development Technologies 6 (1), 83–94.
Li, J, Thielemann, C, Reuning, U.D.J., 2005. Biosensors and Bioelectronics 20 (7), 1333–1340.
Lo, C.M., Keese, C.R., Giaever, I., 1995. Biophysics Journal 69 (6), 2800–2807.
Madara, J.L., Stafford, J., Barenberg, D., Carlson, S., 1988. American Journal of Physiology 254 (3 Pt 1), G416–423.
McAdams, E.T., Lackermeier, A., McLaughlin, J.A., Macken, D., 1995. Biosensors and Bioelectronics 10, 67–74.
Michaelis, S., Rommel, C.E., Endell, J., Goring, P., Wehrspohn, R., Steinem, C., Janshoff, A., Galla, H.J., Wegener, J, 2012. Lab Chip 12 (13), 2329–2336.
Opp, D., Wafula, B., Lim, J., Huang, E., Lo, J.C., Lo, C.M., 2009. Biosensors and Bioelectronics 24 (8), 2625–2629.
Peters, M.F., Scott, C.W., 2009. Journal of Biomolecular Screening 14 (3), 246–255.
Robelek, R., 2009. Bioanalytical Reviews 1 (1), 57–72.
Robelek, R., Wegener, J., 2010. Biosensors and Bioelectronics 25 (5), 1221–1224.
Ruoslahti, E., Pierschbacher, M.D., 1987. Science 238 (4826), 491–497.
Schroder, R., Janssen, N., Schmidt, J., Kebig, A., Merten, N., Hennen, S., Muller, A., Blattermann, S., Mohr-Andra, M., Zahn, S., Wenzel, J., Smith, N.J., Gomeza, J., Drewke, C., Milligan, G., Mohr, K., Kostenis, E., 2010. Nature Biotechnology 28 (9), 943–949.
Scott, C.W., Peters, M.F., 2010. Drug Discovery Today 15 (17–18), 704–716.
Stevenson, B.R., Begg, D.A., 1994. Journal of Cell Science 107 (Pt. 3), 367–375.
Terrettaz, S., Stora, T., Duschl, C., Vogel, H., 1993. Langmuir 9 (5), 1361–1369.
Vala, M., Robelek, R., Bockova, M., Wegener, J., Homola, J., 2013. Biosensors and Bioelectronics 40 (1), 417–421.
Wegener, J., 2003. Cell Junctions. Encyclopedia of Life Sciences. John Wiley & Sons, Ltd, Chichester.
Wegener, J., 2010. Impedance Analysis of Cell Junctions. Wiley-VCH, Weinheim.
Wegener, J., Galla, H.-J., 1996. Chemistry and Physics of Lipids 81, 339–348.
Wegener, J., Hakvoort, A., Galla, H.J., 2000a. Brain Research 853 (1), 115–124.
Wegener, J., Keese, C.R., Giaever, I., 2000b. Experimental Cell Research 259 (1), 158–166.
Wegener, J., Seebach, J., Janshoff, A., Galla, H.J., 2000c. Biophysical Journal 78 (6), 2821–2833.
Wegener, J., Zink, S., Rosen, P., Galla, H., 1999. Pflügers Archiv 437 (6), 925–934.
Yamada, K.M., Kennedy, D.W., 1984. Journal of Cell Biology 99 (1 Pt 1), 29–36.